

Resonant scattering and mode coupling in two-dimensional textured planar waveguides

A. R. Cowan, P. Paddon, V. Pacradouni, and Jeff F. Young

Advanced Materials and Process Engineering Laboratory, Department of Physics and Astronomy, University of British Columbia, 2355 East Mall, Vancouver, British Columbia, Canada V6T 1Z4

Received February 24, 2000; revised manuscript received November 6, 2000; accepted November 6, 2000

A heuristic formalism is developed for efficiently determining the specular reflectivity spectrum of two dimensionally textured planar waveguides. The formalism is based on a Green's function approach wherein the electric fields are assumed to vary little over the thickness of the textured part of the waveguide. Its accuracy, when the thickness of the textured region is much smaller than the wavelength of relevant radiation, is verified by comparison with a much less efficient, "exact" finite difference solution of Maxwell's equations. In addition to its numerical efficiency, the formalism provides an intuitive explanation of Fano-like features evident in the specular reflectivity spectrum when the incident radiation is phase matched to excite leaky electromagnetic modes "attached" to the waveguide. By associating various Fourier components of the scattered field with bare slab modes, the dispersion, unique polarization properties, and lifetimes of these Fano-like features are explained in terms of photonic eigenmodes that reveal the renormalization of the slab modes due to interaction with the two-dimensional grating. An application of the formalism, in the analysis of polarization-insensitive notch filters, is also discussed. © 2001 Optical Society of America

OCIS codes: 230.7390, 350.2770, 310.2790, 260.2110.

1. INTRODUCTION

Periodic dielectric texture can be effectively used to modify and control the optical properties of bulk dielectric hosts at frequencies far removed from any electronic resonances characteristic of that host.¹⁻³ The implications are enormous, especially when the texture extends in two or three dimensions and when the modulation of the refractive index is on the order of unity. Low loss, broadband reflective-antenna platforms have been made at microwave frequencies by machining three-dimensional (3D)-periodic photonic crystals in plexiglass, with lattice constants on the order of centimeters.⁴ Defect states strategically located within such crystals can be used to produce high-*Q* microwave filters.⁵

This concept has even greater implications for the fields of quantum electronics and optoelectronics. Texture on the order of 200–500 nm strongly modifies the photon dispersion in the near-infrared part of the spectrum that is important for optical communications and that is easily accessible with a variety of laser sources. III–V semiconductor heterostructure hosts provide additional opportunities by allowing independent control over both electronic and photonic dispersion: quasi-zero-dimensional (0D) "dots," one-dimensional (1D) "wires," and two-dimensional (2D) "wells" can be produced with a variety of epitaxial growth techniques, and since their characteristic dimensions are on the order of from 2–10 nm, bulk conglomerates of these artificial electronic compounds can then act as hosts for the formation of photonic crystals with texture on length scales approximately 20 to 50 times greater. An example of such a structure has recently been reported by Painter *et al.*,⁶ who fabricated an optically pumped defect-mode laser in a two-dimensionally textured III–V semiconductor waveguide.

Much of the knowledge gained through microwave pho-

tonic band structure work can be extrapolated to nanometer-length scales if electronic resonances can be ignored (Maxwell's equations scale as $\omega\lambda$ for fixed refractive indices). Previous theoretical and modeling work has elucidated the properties of bulk, surface, and defect states in pure 2D and 3D photonic crystals. However, in the near infrared, untextured waveguides of one sort or another are commonly used instead of bulk dielectrics to control the propagation of light (e.g., single-mode optical fibers and slab or ridge waveguides on planar glass or semiconductor substrates). It is therefore of significant interest to understand how strong dielectric texture modifies the dispersion of photons already trapped in waveguides.

Recent experimental work⁷⁻¹⁰ has shown that specular reflectivity spectra from strongly textured waveguides exhibit characteristic Fano-like features when the frequency and in-plane momentum of the incident radiation matches the dispersion of bound or quasi-bound electromagnetic excitations attached to the waveguide. Angular-resolved reflection spectroscopy therefore provides a very powerful means of determining the influence of the 2D texture on the dispersion of the slab modes characteristic of the untextured planar waveguide. Similar features in the specular reflectivity from weak 1D gratings on planar waveguides have been discussed in the context of diffraction theory: There they can be thought of as resonantly enhanced Wood anomalies.¹¹⁻¹³

Various formalisms have been developed to describe the specular reflectivity from 1D and 2D textured waveguides^{12,14-16} and the dispersion of local photonic eigenstates attached to these structures.¹⁷⁻¹⁹ Each of these approaches offers useful insights as to the nature of the photonic excitations characteristic of this geometry. The purpose of this paper is to describe in detail the for-

malism that we developed to successfully model experimental reflection spectra from strongly textured, 80-nm-thick semiconductor membrane waveguides supported on aluminum oxide cladding layers.¹⁰ The merits of this particular formalism include (i) the spectacular level of agreement between its predictions and the experimental spectra referred to above, (ii) its heuristic nature, which stems from the use of an intuitive Green's function, and (related) (iii) its utility in developing a unified understanding of resonant diffraction and photonic band structure in this scattering geometry.

The remainder of the paper is organized as follows. Section 2 elaborates on related work on both 1D and 2D textured waveguides and proceeds to develop the Green's function formalism. Section 3 presents a series of calculated reflectivity spectra that serve to illustrate many of the generic properties of light scattering in this geometry. This section also discusses applications of the model in the design of notch filters. The conclusions are presented in Section 4.

2. THEORY

We develop this formalism as a generalization of our previous treatments of the photonic eigenstates characteristic of planar waveguides containing a weak 1D¹⁸ or 2D¹⁹ surface grating.

The bound and quasi-bound modes in 1D textured waveguides have been studied extensively with coupled-mode theory.^{20,21} When the propagation wave vector of the mode is parallel to the reciprocal lattice vectors of the 1D grating, the eigenmodes of the structure can be expressed as linear combinations of either the transverse electric (TE) or the transverse magnetic (TM) polarized modes bound to the untextured waveguide. The solution of the Maxwell equations then reduces to separate, scalar coupled-mode equations for the TE and TM polarized cases. However, if the modes have some momentum perpendicular to the grating wavevectors in 1D, the true eigenmodes of the textured slab can never be strictly expressed as superpositions of just TE or just TM polarized slab modes: The eigenvalue problem is inherently vector in nature, and scalar coupled mode theory cannot be used to properly describe the electromagnetic excitations.^{18,22}

We recently reported a 2D-vector coupled-mode formalism that retains the intuitive nature of scalar coupled mode theory, but that is valid in the more general situation of obliquely incident radiation and 2D texture.¹⁹ The eigenmodes of the 2D textured waveguide in this formalism are expressed as linear superpositions of both TE and TM polarized slab modes. The importance of properly accounting for depolarization (local field) effects when dealing with electric fields normal to the plane of the waveguides was emphasized.

The 2D-vector coupled-mode formalism¹⁹ was derived from a Green's function solution of the Maxwell equations appropriate to a planar waveguide textured with a weak 2D surface grating in the absence of external (driving) fields. To express the eigenmodes intuitively as a superposition of TE and TM polarized excitations of the untextured waveguide, a resonant pole approximation was made to reduce a general integral equation solution to an eigenvalue problem. That approach provided a transpar-

ent understanding of the physical processes involved in the nontrivial vector coupling that occurs in 2D textured waveguides: The drawback is that the solutions are, typical of coupled-mode theories, not completely self-consistent. This limits its practical application to structures containing weak texture that only slightly perturbs the planar slab modes.

Below we recast the problem in terms of a specular reflectivity calculation. One advantage of this approach is that it remains fully self-consistent while retaining much of the intuitive appeal of the numerically simpler eigenvalue problem. Another significant advantage is that it can be used for direct comparison with experimental results that probe the electromagnetic excitations of these 2D textured waveguides.¹⁰ Although slightly more numerically intensive than the eigenvalue solution, the current approach is still much simpler and more computationally efficient than many other, "exact" solutions of the Maxwell equations in this geometry. "Exact" treatments, such as reported by Whittaker and Culshaw,¹⁵ have the advantage of being able to treat textured layers thicker than the wavelength of radiation. We believe that the heuristic nature of the following Green's function formalism offers important insights that are more difficult to extract with other treatments.

The structure of interest in many optoelectronic devices is the multilayer slab waveguide. We therefore develop a solution for the reflectivity of harmonic plane waves from a dielectric structure consisting of a single planar 2D periodic grating located anywhere within an arbitrary series of homogeneous layers, as schematically illustrated in Fig. 1. The refractive indices and thicknesses of the uniform dielectric layers are typically chosen to support bound slab mode excitations in the absence of the grating. We seek a solution to the inhomogeneous Maxwell equations:

$$\begin{aligned}\nabla \cdot \mathbf{D} &= 0, \\ \nabla \times \mathbf{B} + \frac{i\omega}{c} \mathbf{D} &= 0, \\ \nabla \cdot \mathbf{B} &= 0, \\ \nabla \times \mathbf{E} - \frac{i\omega}{c} \mathbf{B} &= 0.\end{aligned}\quad (1)$$

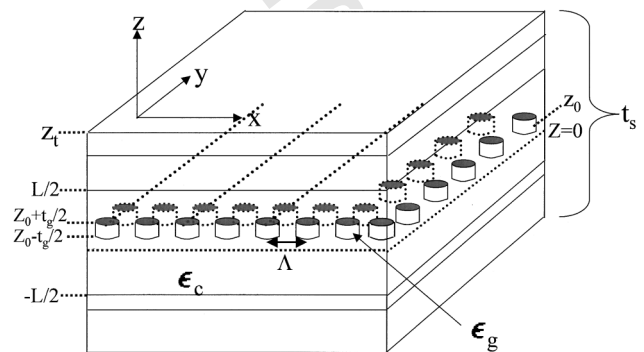


Fig. 1. Schematic of a planar waveguide textured with a 2D planar grating. The grating has thickness t_g , pitch Λ . The dielectric constant of the cylinders is ϵ_g , and they are embedded in a layer of the material that has a dielectric constant ϵ_c .

We are concerned with the linear response of nonmagnetic materials, so we have assumed that all fields oscillate as $\exp(-i\omega t)$, and have set the magnetic permeability to unity, and thus $\mathbf{H} = \mathbf{B}$. The displacement field is given by

$$\mathbf{D} = \mathbf{E} + 4\pi\mathbf{P}^{\text{tot}}, \quad (2)$$

and the total polarization is

$$\mathbf{P}^{\text{tot}}(\omega; \mathbf{r}) = \chi(\omega; \mathbf{r})\mathbf{E}(\omega; \mathbf{r}). \quad (3)$$

To facilitate an intuitive Green's function solution of Eqs. (1), we break up the total linear susceptibility $\chi(\omega; \mathbf{r})$ into two components,

$$\chi(\omega; \mathbf{r}) = \chi_s(\omega; z) + \Delta\chi_g(\omega; z, \boldsymbol{\rho}) \quad (4)$$

where $\chi_s(\omega; z)$ describes the linear response of the untextured slab waveguide and $\Delta\chi_g(\omega; \boldsymbol{\rho}, z)$ represents the deviation from $\chi_s(\omega; z)$ in the textured region, $z_o - t_g/2 < z < z_o + t_g/2$, which we designate with a subscript g . It is subtle but important to note that the grating is represented as a *modification of*, rather than an *addition to*, one of the homogeneous layers that make up the layered slab.

The inhomogeneous Maxwell equations can now be written as

$$\nabla \cdot [\epsilon_s(\omega; z)\mathbf{E}(\omega; \mathbf{r})] = -4\pi\nabla \cdot \Delta\mathbf{P}_g(\omega; \mathbf{r}),$$

$$\nabla \times \mathbf{B}(\omega; \mathbf{r}) + i\tilde{\omega}\epsilon_s(\omega; z)\mathbf{E}(\omega; \mathbf{r}) = -4\pi i\tilde{\omega}\Delta\mathbf{P}_g(\omega; \mathbf{r}),$$

$$\nabla \cdot \mathbf{B}(\omega; \mathbf{r}) = 0,$$

$$\nabla \times \mathbf{E}(\omega; \mathbf{r}) - i\tilde{\omega}\mathbf{B}(\omega; \mathbf{r}) = 0, \quad (5)$$

where $\tilde{\omega} = \omega/c$, $\epsilon_s(\omega; z) = 1 + 4\pi\chi_s(\omega; z)$ and $\Delta\mathbf{P}_g(\omega; \mathbf{r}) = \Delta\chi_g(\omega; \mathbf{r})\mathbf{E}(\omega; \mathbf{r})$.

We seek a solution to Eqs. (5) for the specular reflectivity when a plane wave, $\mathbf{E}_{\text{inc}} \exp[-i(w_o(\beta)z - \boldsymbol{\beta} \cdot \boldsymbol{\rho}) - i\omega t]$ with $w_o(\beta) = (\tilde{\omega}^2 - \beta^2)^{1/2}$, is incident on the 2D textured waveguide from the upper half-space. First, note that a homogeneous solution of Eqs. (5) in the upper half-space, where $z > z_t$ (z_t denotes the top of the structure), is given by

$$\begin{aligned} \mathbf{E}_{\text{UHS}}^{\text{hom}}(\omega; \boldsymbol{\rho}, z) = & \{\exp[-iw_o(\beta)z]\vec{\mathbf{I}} \\ & + \exp[+iw_o(\beta)z]\vec{r}_{wg}(\beta)\} \\ & \cdot \mathbf{E}_{\text{inc}} \exp[i\boldsymbol{\beta} \cdot \boldsymbol{\rho} - i\omega t] \theta(z - z_t) \end{aligned} \quad (6)$$

where θ is the Heaviside function and $\vec{\mathbf{I}}$ is the identity tensor. The Fresnel reflectivity tensor $\vec{r}_{wg}(\beta)$, characteristic of the untextured multilayer, effectively represents the strength of the field radiated into the upper half-space by the polarization induced in the multilayer slab by the incident plane wave. It rigorously takes into account all of the boundary conditions and multiple reflections within the multilayer slab that are implicit in the left-hand side of Eqs. (5).

The total solution that we seek consists of this homogeneous solution, plus the particular solution when the deviation of the polarization in the grating region $\Delta\mathbf{P}_g(\omega; \mathbf{r})$ is considered as a source of fields radiating outward from the grating layer. Because the grating is in general surrounded by dielectric multilayers, the fields originating

from $\Delta\mathbf{P}_g(\omega; \mathbf{r})$ will undergo multiple reflections before eventually escaping into the upper half-space. The reason for expressing the inhomogeneous Maxwell equations in the form of Eqs. (5) is that all of the multiple reflections, and hence the contribution of the additional polarization induced throughout the structure, can be trivially taken into account by using Fresnel reflection tensors, as shown below.

The formal solution for the full specular reflectivity, including the grating response, proceeds as follows. Because we are considering plane-wave excitation with a well-defined in-plane wave vector, $\boldsymbol{\beta}$, and because the 2D periodic texture can be expanded in a Fourier series characterized by a set of 2D reciprocal lattice vectors, $\{\mathbf{G}_m\}$, it is natural to work with the Fourier components of the electric field, as defined by $\mathbf{E}(\omega; \boldsymbol{\rho}, z) = \sum \vec{\mathbf{E}}(\omega; \boldsymbol{\beta} + \mathbf{G}_m, z) \exp[i(\boldsymbol{\beta} + \mathbf{G}_m) \cdot \boldsymbol{\rho}]$, at wave vectors $\boldsymbol{\beta} + \{\mathbf{G}_m\}$. The Green's function approach allows us to determine the Fourier field amplitudes anywhere in space by first determining them self-consistently in the grating (polarization source). First, we recall the Green's function, $\vec{g}_d(\omega, \boldsymbol{\beta}; z, z')$ (d denotes direct), that generates the fields within a uniform dielectric layer, given a localized 2D sheet of polarization $\Delta\mathbf{P}_g(\omega, \boldsymbol{\rho}, z) = \hat{\mathbf{P}}_g(\omega) \delta(z - z') \exp[i\boldsymbol{\beta} \cdot \boldsymbol{\rho}]$, where $\delta(z - z')$ is the Dirac delta function. Second, we derive a Green's function, $\vec{g}_c(\omega, \boldsymbol{\beta}; z, z')$ (c denotes cavity), from \vec{g}_d , using Fresnel reflection tensors. This Green's function generates the field amplitudes within the cavity, the layer containing the grating. It is used to self-consistently find the amplitudes of each Fourier component, $\boldsymbol{\beta} + \{\mathbf{G}_m\}$, of the total electric field in the grating region. Finally, a Green's function, $\vec{g}_{\text{UHS}}(\omega, \boldsymbol{\beta}; z, z')$, that propagates the direct fields into the upper half-space above the structure is used to find the grating's contribution to the specular reflectivity. This is added to the second term of the homogeneous solution, Eq. (6), to find the total specular field.

To find \vec{g}_c , and ultimately the fields in the grating, it suffices to solve Maxwell's equations in the layer containing the grating, the cavity layer, where $\epsilon_s(\omega; z) = \epsilon_c(\omega)$:

$$\epsilon_c(\omega)\nabla \cdot \mathbf{E}(\omega; \boldsymbol{\rho}, z) = -4\pi\nabla \cdot \Delta\mathbf{P}_g(\omega; \boldsymbol{\rho}, z),$$

$$\begin{aligned} \nabla \times \vec{\mathbf{B}}(\omega; \boldsymbol{\rho}, z) + i\tilde{\omega}\epsilon_c(\omega)\mathbf{E}(\omega; \boldsymbol{\rho}, z) \\ = -4\pi i\tilde{\omega}\Delta\mathbf{P}_g(\omega; \boldsymbol{\rho}, z), \end{aligned}$$

$$\nabla \cdot \vec{\mathbf{B}}(\omega; \boldsymbol{\rho}, z) = 0,$$

$$\nabla \times \mathbf{E}(\omega; \boldsymbol{\rho}, z) - i\tilde{\omega}\vec{\mathbf{B}}(\omega; \boldsymbol{\rho}, z) = 0. \quad (7)$$

If this were the only layer in the structure [i.e., if $\epsilon_s(\omega; z) = \epsilon_c(\omega)$ for all z], the solution for the fields radiated away from the grating by any in-plane Fourier component of the polarization, $\Delta\mathbf{P}_g(\omega; \boldsymbol{\kappa}; z')$, could be expressed as²³

$$\mathbf{E}(\omega, \boldsymbol{\kappa}; z) = \int_{-\infty}^{\infty} dz' \vec{g}_d(\boldsymbol{\kappa}; z, z') \cdot \Delta\mathbf{P}_g(\omega, \boldsymbol{\kappa}; z'), \quad (8)$$

where $\vec{g}_d(\boldsymbol{\kappa}; z, z')$ is a Green's function solution of Maxwell's equations in this geometry,²³

$$\begin{aligned} \vec{g}_d(\boldsymbol{\kappa}; z, z') &= \frac{2\pi i \bar{\omega}^2}{w_c(\boldsymbol{\kappa})} \left\{ \theta(z - z') \exp[iw_c(\boldsymbol{\kappa})(z - z')] \right. \\ &\quad \times [\hat{\mathbf{s}}(\boldsymbol{\kappa})\hat{\mathbf{s}}(\boldsymbol{\kappa}) + \hat{\mathbf{p}}_{c+}(\boldsymbol{\kappa})\hat{\mathbf{p}}_{c+}(\boldsymbol{\kappa}) \\ &\quad + \theta(z' - z) \exp[-iw_c(\boldsymbol{\kappa})(z - z')] \\ &\quad \times [\hat{\mathbf{s}}(\boldsymbol{\kappa})\hat{\mathbf{s}}(\boldsymbol{\kappa}) + \hat{\mathbf{p}}_{c-}(\boldsymbol{\kappa})\hat{\mathbf{p}}_{c-}(\boldsymbol{\kappa})] \\ &\quad \left. - \frac{4\pi}{\epsilon_c} \delta(z - z') \hat{\mathbf{z}}\hat{\mathbf{z}}, \right. \end{aligned} \quad (9)$$

where $\delta(z - z')$ is the Dirac delta function and $w_c(\boldsymbol{\kappa}) = (\bar{\omega}^2 \epsilon_c - \boldsymbol{\kappa}^2)^{1/2}$. The ω dependence of ϵ_c has been suppressed to simplify notation. The unit vectors $\hat{\mathbf{s}}(\boldsymbol{\kappa})$ and $\hat{\mathbf{p}}_{c\pm}(\boldsymbol{\kappa})$ define the s - and p -polarization directions. They are

$$\hat{\mathbf{s}}(\boldsymbol{\kappa}) = \hat{\boldsymbol{\kappa}} \times \hat{\mathbf{z}}, \quad (10)$$

$$\hat{\mathbf{p}}_{c\pm}(\boldsymbol{\kappa}) = \frac{\boldsymbol{\kappa} \hat{\mathbf{z}} \mp w_c(\boldsymbol{\kappa}) \hat{\boldsymbol{\kappa}}}{\bar{\omega} \sqrt{\epsilon_c}}. \quad (11)$$

The $\theta(z - z')$ term in Eq. (9) describes waves propagating upward from the polarization source located at z' , and the $\theta(z' - z)$ term describes waves propagating downward. The $\hat{\mathbf{z}}\hat{\mathbf{z}}$ term is due to the $\nabla \cdot \Delta \mathbf{P}_g(\omega; \boldsymbol{\rho}, z)$ term in Maxwell's equations and describes the depolarization effects of the grating.

If the polarization sheet is embedded between two multilayer dielectrics, each of the outward propagating solutions in \vec{g}_d will undergo multiple reflections within the grating cavity. Since the s - and p -polarized components of the field are explicit within the Green's function, the effect of the multilayer stacks can be incorporated with the use of Fresnel coefficients.²³ We describe the reflectivity (as seen from the grating cavity) from the multilayer dielectrics above and below the cavity with the Fresnel coefficients r_{up} and r_{down} , respectively. The multiple reflections generate an infinite series that can be summed to find the Green's function in the layer containing the grating \vec{g}_c :

$$\begin{aligned} \vec{g}_c(\boldsymbol{\kappa}, z, z') &= \frac{2\pi i \bar{\omega}^2}{w_c(\boldsymbol{\kappa})} \left\{ \left[\theta(z - z') \exp[iw_c(\boldsymbol{\kappa})(z - z')] + \theta(z' - z) \exp[-iw_c(\boldsymbol{\kappa})(z - z')] \right] \right. \\ &\quad + (r_{s_{\text{up}}} \exp[-iw_c(\boldsymbol{\kappa})(z + z' - L)] + r_{s_{\text{down}}} \exp[iw_c(\boldsymbol{\kappa})(z + z' + L)] \\ &\quad + r_{s_{\text{up}}} r_{s_{\text{down}}} \{ \exp[iw_c(\boldsymbol{\kappa})(z - z' + 2L)] + \exp[-iw_c(\boldsymbol{\kappa})(z - z' - 2L)] \}) \frac{1}{D_s} \left. \right] \hat{\mathbf{s}}(\boldsymbol{\kappa})\hat{\mathbf{s}}(\boldsymbol{\kappa}) \\ &\quad + \left\{ \theta(z - z') \exp[iw_c(\boldsymbol{\kappa})(z - z')] + \frac{r_{p_{\text{up}}} r_{p_{\text{down}}} \exp[iw_c(\boldsymbol{\kappa})(z - z' + 2L)]}{D_p} \right\} \hat{\mathbf{p}}_{c+}(\boldsymbol{\kappa})\hat{\mathbf{p}}_{c+}(\boldsymbol{\kappa}) \\ &\quad + \left\{ \theta(z' - z) \exp[-iw_c(\boldsymbol{\kappa})(z - z')] + \frac{r_{p_{\text{up}}} r_{p_{\text{down}}} \exp[-iw_c(\boldsymbol{\kappa})(z - z' - 2L)]}{D_p} \right\} \hat{\mathbf{p}}_{c-}(\boldsymbol{\kappa})\hat{\mathbf{p}}_{c-}(\boldsymbol{\kappa}) \\ &\quad + \frac{1}{D_p} [r_{p_{\text{up}}} \exp[-iw_c(\boldsymbol{\kappa})(z + z' - L)] \hat{\mathbf{p}}_{c-}(\boldsymbol{\kappa})\hat{\mathbf{p}}_{c+}(\boldsymbol{\kappa}) + r_{p_{\text{down}}} \exp[iw_c(\boldsymbol{\kappa})(z + z' + L)] \hat{\mathbf{p}}_{c+}(\boldsymbol{\kappa})\hat{\mathbf{p}}_{c-}(\boldsymbol{\kappa})] \\ &\quad \left. - \frac{4\pi}{\epsilon_c} \delta(z - z') \hat{\mathbf{z}}\hat{\mathbf{z}}, \right. \end{aligned} \quad (12)$$

where L is the thickness of the layer containing the grating,

$$D_{s,p} = 1 - r_{s,p_{\text{up}}} r_{s,p_{\text{down}}} \exp[iw_c(\boldsymbol{\kappa})2L] \quad (13)$$

and r_s, r_p are the Fresnel reflection coefficients for s - and p -polarized light, respectively.

The Green's function $\vec{g}_c(\boldsymbol{\kappa}; z, z')$ defined for z in the grating layer gives the electric field generated in the grating layer at z due to the polarization sheet oscillating as $\exp(-i\omega t + i\boldsymbol{\kappa} \cdot \boldsymbol{\rho})$ at z' and all of the polarization it induces in the surrounding multi-layer. This Green's function is completely general; it accounts for gratings located anywhere within the multilayer structure.

For a periodic grating, $\Delta \chi_g(\omega, \mathbf{r})$ can be expressed as a Fourier series

$$\Delta \chi_g(\omega, \mathbf{r}) = \sum_m \chi_{\mathbf{G}_m}(\omega, z) \exp(i\mathbf{G}_m \cdot \boldsymbol{\rho}), \quad (14)$$

where $\{\mathbf{G}_m\}$ is the set of reciprocal lattice vectors of the grating. Substituting this into Eq. (8), we can write the fields radiated by the grating as a sum over the Fourier components of the periodic grating. We then find the solution of Eqs. (7) for the fields in the grating cavity, with in-plane momentum equal to the incident field's in-plane momentum, to be

$$\begin{aligned} \mathbf{E}_c(\omega, \boldsymbol{\beta}; z) &= \mathbf{E}_c^{\text{hom}}(\omega, \boldsymbol{\beta}; z) + \int_{-L/2}^{L/2} dz' \vec{g}_c(\boldsymbol{\beta}; z, z') \\ &\quad \times \sum_m \chi_{\mathbf{G}_m}(\omega; z') \mathbf{E}_c(\omega, \boldsymbol{\beta} - \mathbf{G}_m; z'), \end{aligned} \quad (15)$$

where $\mathbf{E}_c^{\text{hom}}$ is the solution of Maxwell's equations in the grating cavity, Eqs. (7), with $\Delta \mathbf{P}_g = 0$. Note that the polarization in the grating $\Delta \mathbf{P}_g(\omega, \boldsymbol{\beta}; z')$ is given by, $\Delta \mathbf{P}_g(\omega, \boldsymbol{\beta}; z') = \sum_m \chi_{\mathbf{G}_m}(\omega; z') \mathbf{E}_c(\omega, \boldsymbol{\beta} - \mathbf{G}_m; z')$ for z' in the grating layer. Equations similar to Eq. (15) can be

written for each Fourier component of the field, $\boldsymbol{\beta} + \{\mathbf{G}_m\}$, but $\mathbf{E}_c^{\text{hom}}(\omega, \boldsymbol{\beta}; z)$ is nonzero only for the specular component. From Eq. (15) one can clearly see that the effect of the grating is to couple together Fourier components of the field that differ by \mathbf{G}_m and that the strength of this coupling is described by $\chi_{\mathbf{G}_m}(\omega; z)$.

Once Eq. (15) is solved for all the Fourier components of \mathbf{E} in the grating, the fields anywhere can be obtained simply by finding $\vec{g}(\boldsymbol{\beta}; z, z')$ for z in the region of interest. For this specular reflectivity calculation the fields above the structure are given by an equation similar to Eq. (15). The function \vec{g}_c is replaced by a new Green's function, \vec{g}_{UHS} valid above the structure, so that

$$\begin{aligned} \mathbf{E}_{\text{UHS}}(\omega, \boldsymbol{\beta}; z_{\text{above}}) &= \mathbf{E}_{\text{UHS}}^{\text{hom}}(\omega, \boldsymbol{\beta}; z_{\text{above}}) \\ &+ \int_{-L/2}^{L/2} dz' \vec{g}_{\text{UHS}}(\boldsymbol{\beta}; z_{\text{above}}, z') \\ &\cdot \Delta \mathbf{P}_g(\omega, \boldsymbol{\beta}; z'), \end{aligned} \quad (16)$$

where z_{above} denotes a point above the layered structure. The Green's function $\vec{g}_{\text{UHS}}(\boldsymbol{\beta}; z_{\text{above}}, z')$ describes waves that emanate from the polarization at z' and are transmitted out of the top of the structure. It is derived in a similar way as before: by summing the infinite series in Fresnel coefficients which arises due to the multiple reflections within the slab. It is given by

$$\begin{aligned} \vec{g}_{\text{UHS}}(\boldsymbol{\beta}, z_{\text{above}}, z') &= \frac{2\pi i \tilde{\omega}^2}{w_c(\boldsymbol{\beta})} \exp[iw_o(\boldsymbol{\beta})(z_{\text{above}} - z_t)] \\ &\times \exp[iw_c(\boldsymbol{\beta})(L/2 - z')] \\ &\times \left(\frac{t_{s,\text{up}}}{D_s} \{1 + r_{s,\text{down}} \exp[iw_c(\boldsymbol{\beta})(L \right. \\ &+ 2z')]\} \hat{\mathbf{s}}(\boldsymbol{\beta}) \hat{\mathbf{s}}(\boldsymbol{\beta}) \\ &+ \frac{t_{p,\text{up}}}{D_p} \{\hat{\mathbf{p}}_{c+}(\boldsymbol{\beta}) \tilde{\mathbf{p}}_{c+}(\boldsymbol{\beta}) \\ &+ \hat{\mathbf{p}}_{c+}(\boldsymbol{\beta}) \hat{\mathbf{p}}_{c-}(\boldsymbol{\beta}) r_{p,\text{down}} \\ &\left. \times \exp[iw_c(\boldsymbol{\beta})(L + 2z')]\} \right), \end{aligned} \quad (17)$$

where $t_{s,p,\text{up}}$ is the Fresnel transmission coefficient for the layers above the grating cavity and z_t denotes the top of the structure.

To generalize and simplify notation, we write Eq. (15) for z in the grating cavity and for all Fourier field components as

$$\begin{aligned} \mathbf{E}_{(c)n}(z) &= \mathbf{E}_{(c)n}^{\text{hom}}(z) \\ &+ \int_{-L/2}^{L/2} dz' \vec{g}_{(c)n}(z, z') \sum_m \chi_{nm}(z') \mathbf{E}_{(c)m}(z'), \end{aligned} \quad (18)$$

where the ω dependence has been suppressed, the wave vector has been denoted by a subscript, i.e., $\mathbf{E}_c(\omega, \boldsymbol{\beta} - \mathbf{G}_m, z) = \mathbf{E}_{(c)m}(z)$, and $\chi_{nm}(z)$ is the Fourier coefficient

of the grating susceptibility that couples the m th field component to the n th one.

To this point no approximations have been made. Thus the infinite system of equations implied in Eq. (18) gives an exact, self-consistent solution for the fields within the layer containing the grating, with the required Green's function given by Eq. (12). Once this solution in the grating region is found, the infinite set of equations, of which Eq. (16) is one, gives an exact solution for the corresponding fields reflected into the upper half-space.

In order to transform the system of integral Eq. (18) into a system of algebraic equations, we now make some simplifying assumptions. If the grating thickness is much less than the wavelength of light in the material, i.e., $t_g \ll 2\pi/(\tilde{\omega}\sqrt{\epsilon_g})$, then the field intensity will be approximately constant over the grating. We can then replace $\mathbf{E}_{(c)m}(z')$ with the field at the center of the grating, $\mathbf{E}_{(c)m}(z_o)$, where z_o denotes the center of the grating. Furthermore, for a symmetric grating, (i.e., the profile of texture has vertical side walls) χ_{nm} is independent of z and thus can be taken outside of the integral in Eq. (18). With this approximation, the solution for the field at the center of the grating, z_o , is

$$\mathbf{E}_n(z_o) = \mathbf{E}_n^{\text{hom}}(z_o) + \vec{I}_n(z_o) \sum_m \chi_{nm} \mathbf{E}_m(z_o), \quad (19)$$

where $\vec{I}_n(z_o)$ is the Green's function integrated over the thickness of the grating:

$$\vec{I}_n(z_o) = \int_{z_o - t_g/2}^{z_o + t_g/2} \vec{g}_{(c)n}(z_o, z') dz'. \quad (20)$$

Since χ_{nm} is nonzero only in the grating, the integral limits reduce to those in Eq. (20). We have dropped the subscript (c), referring to the grating cavity, as it is implied by specifying that $z = z_o$, z_o always refers to the center of the grating.

The second simplification is to consider a finite number, N , of Fourier components of the field. The infinite set of equations implied in Eq. (19) can then be written in terms of a $3N$ component vector, \vec{E} , and a $3N \times 3N$ component matrix \vec{M} , as

$$\vec{E}(z_o) = \vec{E}^{\text{hom}}(z_o) + \vec{M}(z_o) \cdot \vec{E}(z_o). \quad (21)$$

Here $\vec{M}(z_o) = \vec{I}(z_o) \cdot \vec{\chi}$, where \vec{I} and $\vec{\chi}$ are also $3N \times 3N$ component matrices. \vec{I} is composed of N different 3×3 matrices, the \vec{I}_n from Eq. (19), along the diagonal. $\vec{\chi}$ is a dense set of 3×3 matrices where each has the structure of the identity matrix scaled by the $\chi_{n,m}$ in Eq. (19). Equation (21) is the self-consistent solution for the fields in the grating generated by polarization throughout the entire structure, in response to all nonzero polarization sources. This expression can be manipulated to give the total field in the grating in matrix form as

$$\vec{E}(z_o) = (\mathbf{1} - \vec{M}(z_o))^{-1} \vec{E}^{\text{hom}}(z_o). \quad (22)$$

Upon carrying out analogous notation simplification and approximations to Eq. (16), we can write that infinite set of equations for the fields at the surface of the structure z_t as

$$\vec{E}(z_t) = \vec{E}(z_t) + \vec{N}(z_t)\vec{E}(z_o). \quad (23)$$

Here $\vec{E}(z_t)$, and $\vec{E}(z_t)$ are $3N \times 1$ column matrices of the field components, and $\vec{N}(z_t) = \vec{L}(z_t) \cdot \vec{\chi}$, where $\vec{L}(z_t)$, and $\vec{\chi}$ are $3N \times 3N$ component matrices \vec{L} is composed of N different 3×3 matrices \vec{L}_n along the diagonal, where \vec{L}_n is analogous to \vec{I}_n in Eq. (20) with $\vec{g}_{(cn)}$ replaced by $\vec{g}_{(UHS)n}$. $\vec{\chi}$ is the same matrix as described above. Again, we have dropped the subscript (UHS) in Eq. (23), as it is implied by $z = z_t$.

Substituting Eq. (22) into Eq. (23), we find the solution for the field at the top of the structure z_t in matrix form to be

$$\vec{E}(z_t) = \vec{E}(z_t) + \vec{N}(z_t)(1 - \vec{M}(z_o))^{-1} \vec{E}(z_o), \quad (24)$$

where $\vec{E}(z_t)$ is given by Eq. (6) written as a $3N \times 1$ component vector. Equation (24) gives the field above the structure produced by the polarization in the grating acting on the full multilayer structure and from all other sources. This equation is the general self-consistent solution of our formalism. The field $\vec{E}(z_t)$ contains all N Fourier components included in the calculation, and thus Eq. (24) can be used to calculate the field scattered off of the grating into each Fourier component, N th-order scattering. In this paper we will focus on the specularly reflected field from the structure. This field is the zeroth-order component (zeroth-order scattering) of the N th-order vector $\vec{E}(z_t)$ and includes only the reflected component of the homogeneous solution, \vec{E}_{UHS} . Thus the total specularly reflected field, \vec{E}_{SR} , from the structure, when a field \vec{E}_{inc} is incident from above, is

$$\vec{E}_{SR}(z_t) = \{N(z_t)[1 - M(z_o)]^{-1} \vec{E}(z_o)\}_{\text{specular}} + \vec{r}_{wg}(z_t)\vec{E}_{inc}(z_t). \quad (25)$$

Equation (25) is a self-consistent solution for the specular reflectivity from an arbitrary multilayer slab waveguide that contains one 2D periodic textured layer: the two inherent approximations are (i) the field variation over the thickness of the grating layer is neglected, and (ii) a finite number of Fourier components of the in-plane field structure have been retained.

3. EXAMPLE RESULTS

In this section we use the formalism developed in the previous section to illustrate and explain the resonant diffraction properties of waveguides textured with 2D periodic gratings. The results are discussed in terms of the photonic bandstructure of the corresponding modes excited in the vicinity of the waveguide core.

A. Resonant Modes

We first illustrate some of the basic scattering properties of 2D textured waveguides, using calculated reflectivity spectra from a one-layer slab waveguide of thickness t_s , containing a buried square array of cylindrical dielectric perturbations in a layer of thickness $t_g \ll t_s$. The pitch Λ of a square grating is the real space distance between the dielectric scattering centers. The filling fraction is the ratio of the amount of material within the grating, $z_o - t_g/2 < z < z_o + t_g/2$, with dielectric constant ϵ_g to that with dielectric constant ϵ_c . The parameters for this structure are $\Lambda = 500$ nm, $t_s/\Lambda = 0.26$, $t_g/\Lambda = 0.05$, $\epsilon_c = 12.25$, $\epsilon_g = 2.25$, $z_o = 40$ nm, and the filling fraction of the square symmetric grating is 25%. This structure was chosen primarily for pedagogical reasons; we will refer to it as structure 1. The calculation includes nine Fourier components of the field at $\beta = \{\pm\beta_g, 0\}$, $\{0, \pm\beta_g\}$, $\{\pm\beta_g, \pm\beta_g\}$, and $\{0, 0\}$. The specular reflectivity of this structure when excited with an incident plane wave with a fixed in-plane wave vector of $\beta/\beta_g = 0.01\hat{x}$ (which is slightly off of zone center in the X -symmetry direction) is shown in Fig. 2. Many features of this spectrum can be understood in terms of simple kinematics and resonant diffraction into bound modes characteristic of the slab. These features are described first, in Subsection 3.A.1. Other more subtle features are associated with the symmetry and dispersion of the true modes of the complete structure, including the texture. These properties are discussed in Subsection 3.A.2.

1. Kinematic Effects

The specular reflectivity spectrum from an *untextured* multilayer dielectric slab is modulated by the constructive and destructive interference of multiply reflected fields with a unique in-plane wave vector $\beta(\omega)$ for each driving frequency ω . This gives rise to the slowly varying background in the spectrum in Fig. 2. In the presence of a periodic grating with Fourier components $\{\mathbf{G}_m\}$, incident plane waves with in-plane wave vectors $\beta(\omega)$ generate a polarization source at the grating that excites the surrounding layers with fields oscillating at the same frequency, but with in-plane wave vectors $\beta(\omega) + \{\mathbf{G}_m\}$. In

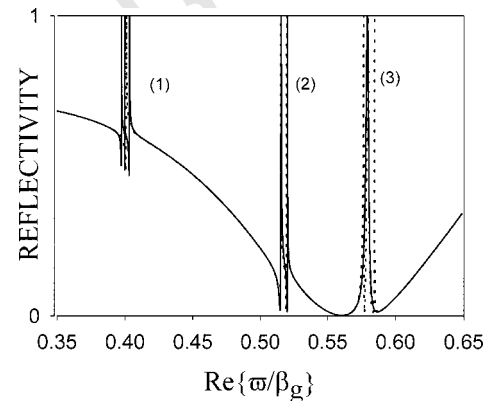


Fig. 2. Reflectivity spectrum at $\beta/\beta_g = 0.01\hat{x}$ for structure 1 described in the text. Solid curve, s -polarized radiation; dotted curve, p -polarized radiation. Each resonance is due to coupling into the radiative component of the renormalized slab modes with (1) the lowest-order TE-like modes, (2) the next-higher-order TE-like modes, and (3) the lowest-order TM-like modes.

most of the examples considered here, and in the resonant diffraction literature, these locally driven fields are ordinarily weak and have little effect on the specular reflectivity spectrum. However, even for a weak perturbation, if one of the $\beta(\omega) + \{\mathbf{G}_m\}$ is close to a wave vector at which the untextured slab supports a bound mode, the amplitude of the corresponding field can become very large. This resonant field influences the specular reflectivity spectrum over a range of frequencies in the vicinity of this phase-matched condition. The sharp features in Fig. 2 correspond to frequencies at which the various Fourier components of the 2D periodic grating add to the incident wave vector $\beta = 0.01\beta_g \hat{x}$ to, effectively, resonantly excite various TE and TM slab modes.

It is evident from Fig. 2 that near zone center the resonant modes are grouped in sets of four. This is a consequence of symmetry in the 2D square reciprocal lattice. Recall that of the nine lowest-order Fourier components of the field, four have $|\beta| \sim \beta_g$. The four resonances labeled (1) in Fig. 2 are due to coupling into four eigenmodes of the textured waveguide that are *predominantly* composed of distinct linear combinations of these four TE-polarized Fourier components of the field. The resonances labeled (2) are the eigenmodes that are composed *primarily* of the TE Fourier components with $|\beta| \sim \sqrt{2}\beta_g$. The set of peaks labeled (3) are made up *primarily* of the four TM-polarized Fourier components with $|\beta| \sim \beta_g$. The TM slab modes are at a higher energy as the effective index for the TM slab modes is less than for TE slab modes. At an even higher energy, one would observe the four eigenmodes resulting from the TM Fourier components at $|\beta| \sim \sqrt{2}\beta_g$, etc.

Figure 3 is a schematic dispersion diagram for modes localized in the vicinity of a weak square grating. It simply illustrates the zone folding that occurs as a result of Bloch's theorem. The insets depict the Fourier components and the wave vectors of each component of the lowest-order eigenmodes. The pure kinematic, or zone folding, effects shown in Fig. 3 predict degeneracies, so that only three features should be evident in groups (1) and (3) and only two features in group (2) of Fig. 2 (by symmetry, group (2) is equivalent to detuning in the M direction, but at higher energy). To understand why there are in fact four distinct modes (as one might anticipate from the insets) in both the X and the M directions, as well as the fact that different modes are only excited by only s - or only p -polarized radiation, it is necessary to go beyond the simple kinematic effects of the 2D grating and consider how it modifies the basic nature of the eigenstates.

2. Mode-Renormalization Effects

The reflectivity spectrum around the set of resonances labeled by (1) in Fig. 2 is shown on an enlarged scale in Fig. 4(a) for a variety of in-plane wave vectors extending 2% of the way to the X point of the Brillouin zone. Note that the sharp, Fano-like features that signify coupling to waveguide modes all rise precisely to unity reflectivity. This has been noted previously by others in the context of 1D and 2D gratings,^{12,16,24} and always occurs when only one of the components of the Bloch state is kinematically allowed to radiate into either cladding region. Note also

that different resonances have quite different linewidths. These linewidths are inversely related to the lifetimes of the associated Bloch states, as limited by the strength of their radiating component. The four modes evident in all of these spectra are primarily TE polarized, although all have some admixture of TM polarization.

It is the lack of translational invariance normal to the textured plane that causes this mixing of TE- and TM-

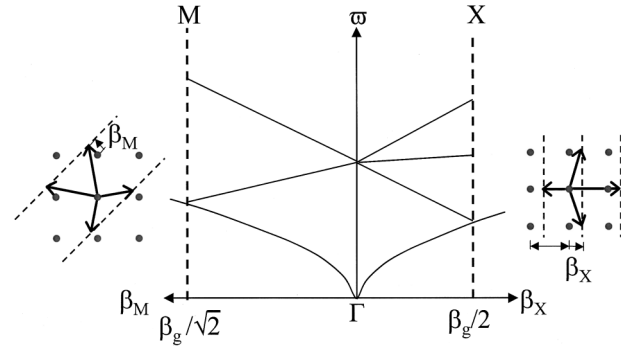


Fig. 3. Schematic plot of the band structure across the first Brillouin zone in the X and M directions for a weak square grating. This plot shows the kinematic coupling (zone folding) of all modes only to the first Brillouin zone. The renormalization effects of the grating, which lead to avoided crossings, and zero slope for the bands at the Brillouin zone boundaries are not described by these purely kinematic effects. The insets show the nine Fourier components and the wave vectors of the eigenmode components with detuning in the X and M directions.

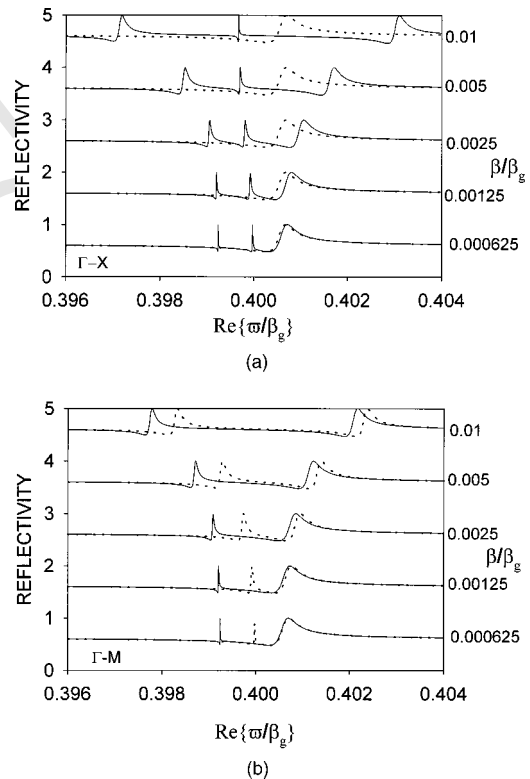


Fig. 4. Reflectivity spectra for increasing $|\beta/\beta_g|$ away from zone center for a square grating (structure 1) with detuning in (a) the X and (b) the M symmetry directions. Solid curve, s -polarized radiation; dotted curve, p -polarized radiation. As resonances approach zone center, their width approaches zero or they become degenerate with opposite polarizations. The different dispersion and lifetime properties of the eigenmodes are evident.

polarized field components. This makes it impossible to label the eigenmodes of the textured waveguide as purely TE or TM. However, we show below that the polarization of the zeroth-order Fourier component of the eigenmodes (the component within the first Brillouin zone) is in fact strictly *s* or *p* polarized along high-symmetry directions. Therefore the polarization of the zeroth-order component of the eigenmodes serves as a good quantum number associated with well-defined selection rules along these high-symmetry directions.

At zone center the two narrow modes become infinitely long lived (true bound modes) and the two broad modes become degenerate. This is a fundamental consequence of the symmetry of the lattice: No isolated mode at the zone center could have a finite lifetime because there can be no preferred polarization of its radiative component. Modes that radiate (have finite lifetimes) at the zone center must be degenerate. It is the degenerate modes that are of interest for application in polarization-insensitive notch filters,¹⁶ as explained in Subsection 3.B.

The fact that the two dispersive bands and one of the less dispersive bands can be excited only by *s*-polarized light, while the other weakly dispersive band can be excited only by *p*-polarized light (despite being primarily TE polarized within the guide), is another consequence of symmetry. Along directions with mirror symmetry, such as the *X* and the *M* directions in the square lattice, all of the Fourier components of the Bloch state that are symmetrically oriented with respect to the propagation direction must be either symmetric or antisymmetric. Away from the zone center, the two dispersive eigenmodes quickly become dominated by a single Fourier component oriented parallel or antiparallel to the direction of propagation. Since they are predominantly TE polarized, the zeroth-order polarization that they drive must radiate *s*-polarized light. The two less dispersive modes quickly become linear superpositions of Fourier field components oriented almost perpendicular to the direction of propagation (see inset to Fig. 3). The symmetric superposition of two TE-polarized Fourier components must, from symmetry, have a net electric field perpendicular to the direction of propagation, and it must therefore also drive a zeroth-order polarization that radiates *s*-polarized light. The antisymmetric superposition results in an electric field oriented parallel to the direction of propagation, and it therefore drives a zeroth-order polarization that radiates with *p* polarization.

To this point we have discussed only detuning from zone center in the *X* direction. The *M* direction is the other direction of high symmetry in the square lattice. Away from the zone center along this direction, *all* of the modes gradually become dominated by a linear superposition of two symmetric or antisymmetric pairs of slab modes oriented at $\sim 45^\circ$ from the propagation direction (see insets to Fig. 3). Figure 4(b) shows the reflectivity spectra for β along the *M* direction. All four modes that evolve from the zone center along the *M* direction of a square lattice exhibit significant dispersion, and they come in pairs, with one having an *s*- and the other having a *p*-polarized radiative component.

Although this discussion has been restricted to the dominant field components of the modes, it in fact applies

to all of the components, which is why the calculations clearly show that each band is excited only by *s*- or only by *p*-polarized radiation.

To summarize the physics of resonant modes attached to planar textured waveguides as investigated with our reflectivity calculation, we note that each reflectivity spectrum effectively probes the dispersion of the eigenmodes along a vertical line in $\tilde{\omega} - \beta$ space. Thus a plot of the value of $\tilde{\omega}/\beta_g$ at each resonance as a function of β yields the dispersion diagram. The dispersion diagram for the square grating, found by plotting $\tilde{\omega}/\beta_g$ for each resonance in Fig. 4(a), is illustrated in Fig. 5. The slope of the dispersion curve for each eigenmode is the group velocity of that mode. In contrast to Fig. 3, near the zone center the group velocity of the eigenmodes is modified owing to the renormalization effects of the index contrast. The extent to which the modified group velocity extends away from the zone center increases with increasing scattering strength (index contrast). Right at the zone center the group velocity is zero, and photonic standing waves result from the highly symmetric coupling of the bare slab modes.

B. Bound Modes

The specular reflectivity spectrum of propagating plane waves thus provides a convenient probe of the photonic dispersion of the leaky modes attached to the porous waveguide. By considering the reflectivity of evanescent waves, it is possible to probe the true bound eigenmodes: modes with $\tilde{\omega}\sqrt{\epsilon_{\text{cladding}}^{\text{max}}} < |\beta|$, where $\epsilon_{\text{cladding}}^{\text{max}}$ is the dielectric constant of the cladding layer with the largest dielectric constant. Instead of appearing as Fano resonances bounded by unity reflectivity, the bound modes are revealed as poles in the specular reflectivity.

As an example, we consider the same structure as in Subsection 3.A (structure 1); but to probe the band structure near the *X* point in the first Brillouin zone boundary, we now incorporate six Fourier components of the field in the model, at $\beta = \{\pm\beta_g/2, 0\}$ and $\{\pm\beta_g/2, \pm\beta_g\}$. Note that now there are no Fourier components of the Bloch states that are phase matched to radiate into the substrate or the vacuum.

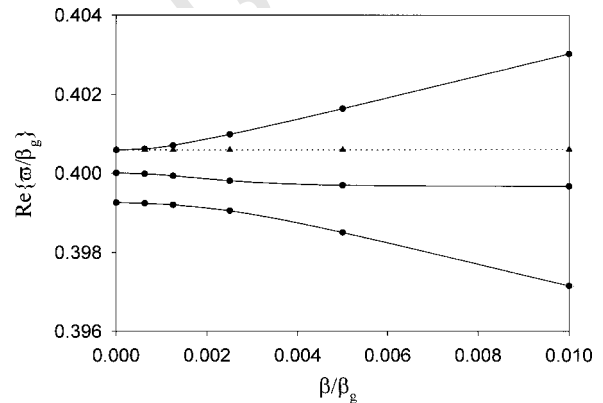


Fig. 5. Dispersion diagram for a square grating in the *X* direction within the first Brillouin zone. Solid curves, *s*-polarized eigenmodes; dotted curve, *p*-polarized eigenmodes. The symbols represent the location of peaks in the first-order diffracted spectra, peaks that correspond to the true resonance frequency of the Fano-like features in Fig. 4(a).

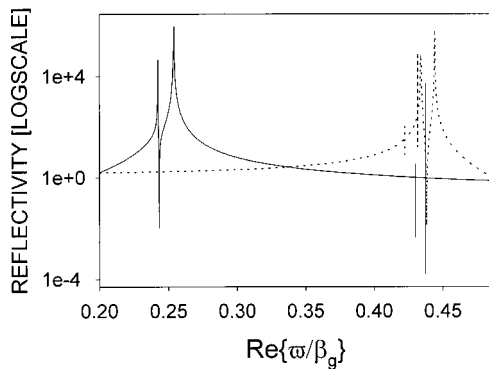


Fig. 6. Reflectivity spectrum near the Brillouin zone boundary ($\beta/\beta_g = 0.485\hat{x}$) for the square grating (structure 1). The true bound modes appear as poles in the specular reflectivity spectrum. Of the four p -polarized modes, the two at lower $\tilde{\omega}$ are TE-like modes and the upper two are the lowest-order TM-like modes.

Figure 6 shows the reflectivity spectrum at $\beta/\beta_g = 0.485\hat{x}$. There are two resonances excited by s -polarized evanescent waves near $\tilde{\omega}/\beta_g \approx 0.25$. These are eigenmodes made up of essentially TE slab modes near $\beta = \{\pm\beta_g/2, 0\}$. The second set of peaks near $\tilde{\omega}/\beta_g \approx 0.43$ consists of six resonances. Two of these are the lowest-order TM-like eigenmodes, consisting of TM slab modes near $\beta = \{\pm\beta_g/2, 0\}$, similar in nature to the s -polarized doublet at lower energy. The other four eigenmodes are composed *primarily* of the TE-like slab modes at $\beta = \{\pm\beta_g/2, \pm\beta_g\}$. Two are excited by s -polarized and two by p -polarized evanescent fields. Note that for this structure, $\epsilon_{\text{cladding}}^{\text{max}} = 1.0$, so it is easy to verify that all of these modes satisfy $\tilde{\omega} < |\beta|$.

As in the previous subsection, we can determine the band structure of the purely bound modes by plotting the location of these poles as a function of β . In this manner our approach reveals the dispersion of both resonant and bound electromagnetic modes throughout the entire Brillouin zone.

C. Accuracy

We demonstrate the accuracy of this Green's-function-based reflectivity calculation when applied to a thin slab, by comparing it with an exact integration of Maxwell's equations.^{7,14} Figure 7 compares the specular reflectivity from the 2D textured slab considered above (structure 1), as calculated with the approach described in Section 2, and use of the exact model. The computation time required for the exact solution was approximately 2000 times longer than for the Green's function approach. In Fig. 7 it is clear that the spectra are in excellent agreement, with respect to both the locations and the widths of the resonances. The center of the gap agrees to within 0.6%, and the gap width to within 7%.

The use of a finite number of Fourier components has some effect on the convergence of our numerical solutions. We have tested the related convergence on a number of semiconductor air/oxide structures with gratings ranging from 0 to 150 nm in thickness; in general, we find that it is sufficient to include up to second-order Fourier components. In particular, for the structure considered here, increasing the number of Fourier components from the

smallest 9 to the smallest 25 shifts the resonances by only 0.015%. The error shown in Fig. 7 is therefore due almost entirely to the thin-grating approximation.

To address further the limitations imposed by the thin-grating approximation, we consider a symmetric waveguide textured with a 1D grating having a filling fraction of 25%, $\epsilon_s = 12.25$, and $\epsilon_g = 1.0$. The inset to Fig. 7 plots the location of the upper and lower edges of the second-order gap as calculated with the Green's function (dashed curve), and the exact (solid curve) methods. It is clear that for thin gratings the two methods agree extremely well. When the waveguide is 250 nm thick, a thickness greater than those that are usually of interest in the context of photonic crystal membranes, the two methods agree to within 4.5% for the upper edge and 0.6% for the lower edge. This demonstrates that it is not possible to specify a simple relationship between the model's accuracy and the grating thickness. For a given structure the accuracy depends on the mode being studied, and different layer structures may result in different errors for a fixed grating thickness.

We can make two further points regarding accuracy. Firstly, for an 80-nm GaAs slab atop a 1.8- μm aluminum oxide cladding layer, the Green's function model reported here has been tested successfully against the measured spectra from a 2D square array of holes that completely penetrated the 80 nm slab (Ref. 10). The pitch and the

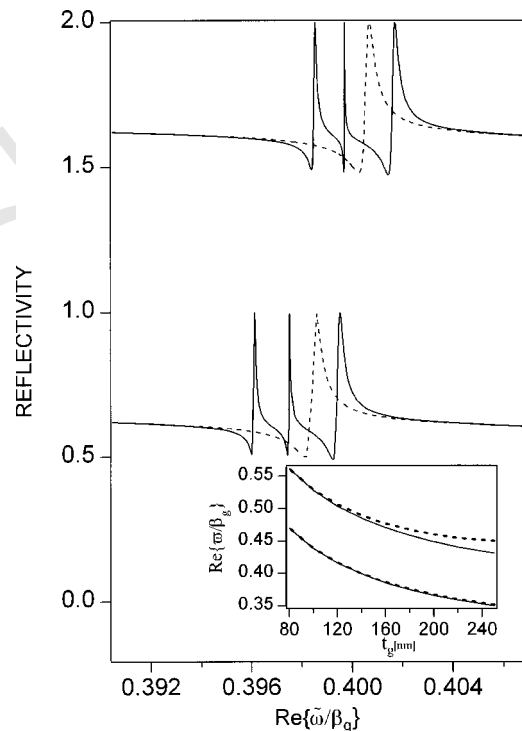


Fig. 7. Reflectivity spectra for structure 1 as calculated with an exact integration of Maxwell's equations (lower plot) and with the approach described in this paper (upper plot). The resonance widths and shape are in excellent agreement. The gap width agrees to within 7%, and the center of the gap agrees to within 0.6%. The inset shows the location of the upper and lower edges of the second-order gap in a 1D textured symmetric waveguide of thickness t_g , $\epsilon_s = 12.25$, $\epsilon_g = 1.0$, and a filling fraction of 25%, as calculated with the Green's function (dashed curves) and exact (solid curves) methods.

resonant-waveguide notch filters. In particular, the resonant, polarization-insensitive reflectivity is associated with coupling to two leaky photonic bands, one *s* and one *p* polarized, that become degenerate at the zone center.

Finally, the accuracy of this simple model has been verified both by comparison with an exact solution of Maxwell's equations when the thickness of the textured layer is much less than the wavelength of interest and by comparison with experimental reflectivity measurements on 2D square gratings etched into GaAs slab waveguides.^{10,25}

ACKNOWLEDGMENTS

This research was funded by the Natural Sciences and Engineering Research Council of Canada, and the Canadian Cable Labs Fund.

REFERENCES

1. S. John, "Strong localization of photons in certain disordered dielectric superlattices," *Phys. Rev. Lett.* **58**, 2486–2489 (1987).
2. E. Yablonovitch, "Inhibited spontaneous emission in solid-state physics and electronics," *Phys. Rev. Lett.* **58**, 2059–2062 (1987).
3. J. D. Joannopoulos, P. R. Villeneuve *et al.*, "Photonic crystals: putting a new twist on light," *Nature* **386**, 143–149 (1997).
4. K. Agi, E. R. Brown, O. B. McMahon, C. Dill III, and K. J. Malloy, "Design of ultrawideband photonic broadband antenna applications," *Electron. Lett.* **30**, 2166–2167 (1994).
5. E. Yablonovitch, T. J. Gmitter, R. D. Meade, A. M. Rappe, K. D. Brommer, and J. D. Joannopoulos, "Donor and acceptor modes in photonic band structure," *Phys. Rev. Lett.* **67**, 3380–3383 (1991).
6. O. Painter, R. K. Lee, A. Scherer, A. Yariv, J. D. O'Brien, P. D. Dapkus, and I. Kim, "Two-dimensional photonic band-gap defect mode laser," *Science* **284**, 1819–1821 (1999).
7. M. Kanskar, P. Paddon, V. Pacradouni, R. Morin, A. Busch, J. F. Young, S. R. Johnson, J. Mackenzie, and T. Tiedje, "Observation of leaky slab modes in air-bridge semiconductor waveguides with a two-dimensional photonic lattice," *Appl. Phys. Lett.* **70**, 1438–1440 (1997).
8. V. N. Astratov *et al.*, "Photonic band-structure effects in the reflectivity of periodically patterned waveguides," *Phys. Rev. B* **60**, R16255–R16258 (1999).
9. V. N. Astratov *et al.*, "Resonant coupling of near-infrared radiation to photonic band structure waveguides," *J. Lightwave Technol.* **17**, 2050–2056 (1999).
10. V. Pacradouni, J. Mandeville, A. R. Cowan, P. Paddon, and J. F. Young, "Photonic bandstructure of dielectric membranes periodically textured in two dimensions," *Phys. Rev. B* **62**, 4204–4207 (2000).
11. S. M. Norton, T. Erdogan, and G. Michael Morris, "Coupled-mode theory of resonant-grating filters," *J. Opt. Soc. Am. A* **14**, 629–639 (1997).
12. S. Tibuleac and R. Magnusson, "Reflection and transmission guided-mode resonance filters," *J. Opt. Soc. Am. A* **14**, 1617–1626 (1997).
13. T. Tamir and S. Zhang, "Resonant scattering by multilayered dielectric gratings," *J. Opt. Soc. Am. A* **14**, 1607–1616 (1997).
14. J. F. Young, P. Paddon, V. Pacradouni, T. Tiedje, and S. Johnson, "Photonic lattices in semiconductor waveguides," in *Future Trends in Microelectronics*, S. Luryi, J. Xu, and A. Zaslavsky, eds. (Wiley, Toronto, 1999), pp. 423–432.
15. D. M. Whittaker, and I. S. Culshaw, "Scattering-matrix treatment of patterned multilayer photonic structures," *Phys. Rev. B* **60**, 2610–2618 (1999).
16. S. Peng and G. M. Morris, "Resonant Scattering from two-dimensional gratings," *J. Opt. Soc. Am. A* **13**, 993–1005 (1996).
17. D. M. Atkin *et al.*, "Photonic band structure of guided Bloch modes in high index films fully etched through with periodic microstructure," *J. Mod. Opt.* **43**, 1035–1053 (1996).
18. P. Paddon and J. F. Young, "Simple approach to coupling in textured planar waveguides," *Opt. Lett.* **23**, 1529–1531 (1998).
19. P. Paddon and J. F. Young, "Two-dimensional vector-coupled-mode theory for textured planar waveguides," *Phys. Rev. B* **61**, 2090–2101 (2000).
20. A. Yariv, "Coupled-mode theory for guided wave optics," *IEEE J. Quantum Electron.* **QE-9**, 919–933 (1973).
21. W. Streifer *et al.*, "Coupled wave analysis of DFB and DBR lasers," *IEEE J. Quantum Electron.* **QE-13**, 134–141 (1977).
22. L. A. Weller-Brophy and D. G. Hall, "Local normal mode analysis of guided mode interactions with waveguide gratings," *J. Lightwave Technol.* **6**, 1069–1082 (1988).
23. J. E. Sipe, "New Green-function formalism for surface optics," *J. Opt. Soc. Am. B* **4**, 481–489 (1987).
24. S. Peng and G. M. Morris, "Experimental investigation of resonant grating filters based on two-dimensional gratings," in *Diffraction and Holographic Optics Technology III*, I. Cindrich and S. H. Lee, eds, Proc. SPIE **2689**, 90–94 (1996).
25. V. Pacradouni, A. R. Cowan, J. Mandeville, P. Paddon, and J. F. Young, "Dispersion and lifetimes of leaky modes attached to 2D waveguide-based photonic crystals: experiment and theory," post deadline conference proceedings, 1999 OSA Annual Meeting, Santa Clara, California, September 26–30, 1999.
26. A. R. Cowan and J. F. Young, to be published.